CrossMark

ORIGINAL ARTICLE

The influence of the diamond wheel grinding process on the selected properties of boron nitride dispersion in cemented carbide (BNDCC) composites

Barbara Staniewicz-Brudnik[1] · Małgorzata Karolus[1] · Elżbieta Bączek[1] ·
Grzegorz Skrabalak[1] · Jolanta Laszkiewicz-Łukasik[1]

Abstract The paper presents the results of research into the influence of the process of grinding boron nitride dispersed cemented carbide (BNDCC) composite using diamond wheel with vitrified bond on the selected properties of this composite. Cutting tools of BNDCC composite were manufactured using several machining operations. At first stage, they were EDM (electrical discharge machining) wire cut from tablets and later on ground with diamond wheels (which removed the "white layer" produced by EDM cutting). Rake and flank faces of prepared cutting tools were examined by microscopic, topographic, and surface analytical techniques before and after grinding. The paper presents comparative results of BNDCC tools and tools made of H10S cemented carbide. Values of the grinding efficiency parameters, Q_w, average material removal rate of grinding, Q'_w, average material removal rate per unit active grinding wheel for the two materials, were similar, indicating an insignificant effect of introduction of the harder BN phase into WCCo on

these parameters. R_a, surface roughness of flank face, was 0.040 μm for BNDCC composite and 0.51 μm for H10S after grinding, compared to 1.14 and 1.30 μm, respectively, before grinding. WC residual stress measurements in the flank faces of BNDCC tools were inconclusive; in the flank faces, the stresses were compressive, decreasing, e.g., from − 230 to − 1670 MPa after grinding. For the H10S tools, there was no comparable effect. The results also indicate that the vitrified bonded diamond abrasive wheel used is effective in grinding WCCo and BNDCC cutting tools.

Keywords Sintering · Composites · X-ray methods · Wear resistance · Glass ceramics

✉ Małgorzata Karolus
karolus@us.edu.pl

Barbara Staniewicz-Brudnik
barbara.brudnik@ios.krakow.pl

Elżbieta Bączek
elzbieta.baczek@ios.krakow.pl

Grzegorz Skrabalak
grzegorz.skrabalak@ios.krakow.pl

Jolanta Laszkiewicz-Łukasik
jolanta.laszkiewicz@ios.krakow.pl

[1] Institute of Advanced Manufacturing Technology, Wroclawska 37A, 30-011 Cracow, Poland

1 Introduction

When machining abrasion-resistant materials such as composites of metal-ceramic matrix with non-ferrous metals (in particular aluminum and titanium) and its alloys reinforced with hard particles and composites of plastics reinforced with glass fibers, cemented carbide tools are being replaced by considerably more expensive, but more abrasion-resistant polycrystalline diamond (*PCD*) tools [1–3]. The wear resistance of cemented carbides can be significantly increased, while retaining their high fracture toughness, by replacing part of the carbide phase with cubic boron nitride grains as a dispersive phase. This composite can be produced with method of pulse plasma sintering (*PPS*) [4–6]. This method allows to carry out the sintering process at a lower temperature and in shorter time than the conventional methods for preparing WCCo composite. Composites such as cubic boron nitride dispersed in cemented carbide (BNDCC) are

Table 1 Properties of the ceramic binder used for diamond grinding wheels (results are averaged values of five grinding attempts)

Binder properties	"Ba23 bis" binder
Wettability to substrate graphite [deg]	38 ± 2
Microhardness [GPa]	5.9 ± 0.12
Flexural strength [MPa]	100 ± 2.71
Young modulus [MPa]	89 ± 3.1
TCE coefficient [10^{-6} 1/deg]	4.9 ± 0.06

characterized by higher hardness, wear resistance, the same high resistance to cracking than sintered (cemented) carbide, and higher coefficient of thermal conductivity which improved working condition for tool by lowering the temperature in cut zone. The grinding process of BNDCC composites required special diamond abrasive tools containing ceramic (vitrified) binders [7, 8] dedicated to processing of these materials.

The effectiveness of using a vitrified bond indicates the selection of properties such as good wetting of the diamond by binder [9], similar or identical values of coefficient of the linear thermal expansion of binder and diamond, high microhardness, and high Young modulus of binder. These properties induced the abrasive grains in the ring working up to self-sharpening as well as preventing from adhesion to the workpiece during grinding process. These properties are
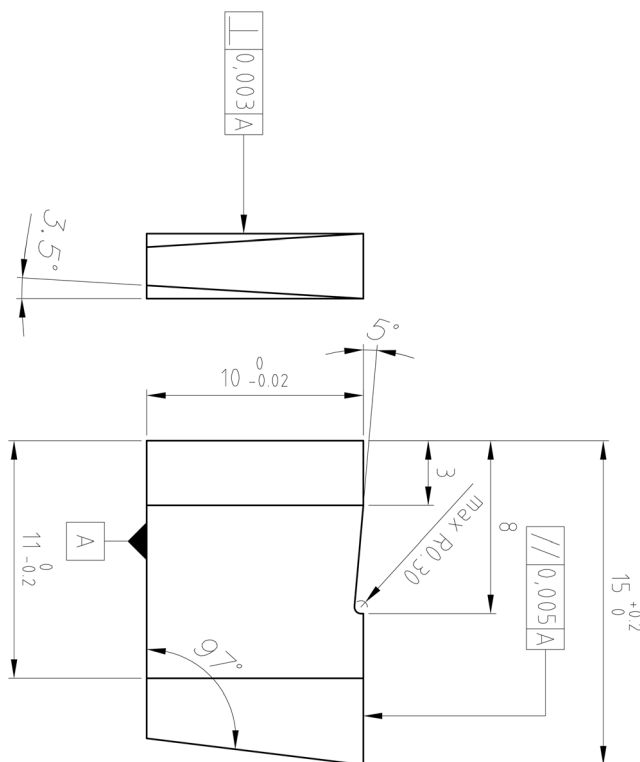

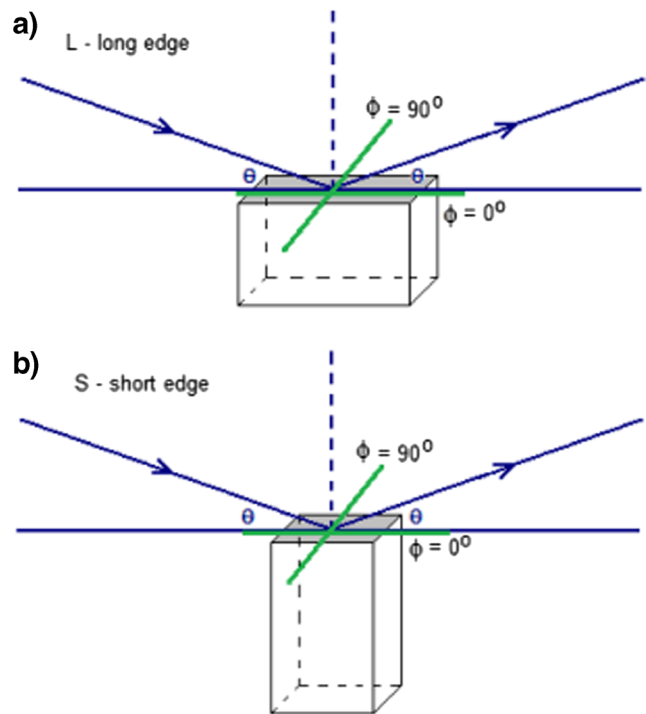**Fig. 1** The scheme of edge of BNDCC composite

Fig. 2 The scheme of the measurement geometry of testing samples: **a** long edge (rake face), *L*, and **b** short edge (flank face), *S*

characterized by a ceramic binder based on Al_2O_3-SiO_2-Na_2O-B_2O_3-BaO system glass (Table 1).

Our diamond grinding wheel with ceramic binder in addition to multi-component system glass contained molybdenum disulfide MoS_2 and bismuth oxide Bi_2O_3. Molybdenum disulfide fulfills the role of a solid lubricant resulting from its layered structure. The S-Mo-S layers formed the loosely packages bonded linked together but at the same time they combined a strong bond with a dominant share of covalent. The role of bismuth oxide was primarily to produce a reinforcing thin submicron film around the diamond grains reinforcing connection with the binder with a binder.

The results of literature and technical catalogues of diamond grinding wheel producers survey show that the diamond grinding tools are characterized by such unique

Table 2 Average parameters (Q_w and Q'_w) with standard deviation of the grinding process of BNDCC composite by *D25* grinding wheel

BNDCC	Working engagement g [mm/double stroke of the table]	Average material removal rate of grinding $Q_w \times 10^{-2}$ [mm³/s]	Average material removal rate per unit active grinding wheel $Q'_w \times 10^{-2}$ [mm³/mm s]
Rake face area	0.01	1.032 ± 0.063	0.103 ± 0.006
	0.02	2.172 ± 0.322	0.217 ± 0.032
Flank face area	0.01	1.224 ± 0.229	0.122 ± 0.023
	0.02	2.55 ± 0.202	0.255 ± 0.020

Table 3 Average parameters (Q_w and Q'_w) with standard deviation of the grinding process of H10S composite by *D25* grinding wheel

H10S	Working engagement g [mm/double stroke of the table]	Average material removal rate of grinding $Q_w \times 10^{-2}$ [mm³/s]	Average material removal rate per unit active grinding wheel $Q'_w \times 10^{-2}$ [mm³/mm s]
Rake face area	0.01	1.094 ± 0.150	0.109 ± 0.0150
	0.02	2.226 ± 0.26	0.223 ± 0.026
Flank face area	0.01	1.276 ± 0.115	0.128 ± 0.0011
	0.02	2.542 ± 0.183	0.254 ± 0.018

Table 5 Average parameters (Q_w and Q'_w) with standard deviation of the grinding process of H10S composite by *D46* grinding wheel

H10	Working engagement g [mm/double stroke of the table]	Average material removal rate of grinding $Q_w \times 10^{-2}$ [mm³/s]	Average material removal rate per unit active grinding wheel $Q'_w \times 10^{-2}$ [mm³/mm s]
Rake face area	0.01	1.098 ± 0.087	0.110 ± 0.009
	0.02	2.178 ± 0.212	0.218 ± 0.021
Flank face area	0.01	1.272 ± 0.355	0.127 ± 0.035
	0.02	2.506 ± 0.271	0.251 ± 0.027

properties. Among others, the most commonly used concerns are as follows: volume fraction (ranging from C120 to C480); structure, hardness and porosity; and a considerable capacity for both self-sharpening and shaping by the conventional method.

Presented research focuses on the impact of grinding process (with diamond wheels built with dedicated ceramic binder) on residual stresses of their own flank and rake face area of machined cutting tools of H10S and BNDCC composites.

2 Materials

Manufacturing of BNDCC cutting tools used in the study includes several shaping stages and machining processes. At first stage, raw material (supplied by the Warsaw University of Technology in the form of tablets of 4.1 mm thick with diameter of 19 mm) are machined with wired electrodischarge cutting (WEDM)—for surface waviness smoothing and cutting of tool geometry leaving ~0.2 mm in each dimension for finishing operations. The second stage of machining concerns grinding of prepared sub-products: flat side surfaces grinding and grinding of tool edges.

For WEDM process, the wire-cutting machine of the Institute design—EDM-EWIOS40—was used. WEDM

Table 4 Average parameters (Q_w and Q'_w) with standard deviation of the grinding process of BNDCC composite by *D46* grinding wheel

BNDCC	Working engagement g [mm/double stroke of the table]	Average material removal rate of grinding $Q_w \times 10^{-2}$ [mm³/s]	Average material removal rate per unit active grinding wheel $Q'_w \times 10^{-2}$ [mm³/mm s]
Rake face area	0.01	1.028 ± 0.145	0.103 ± 0.0145
	0.02	2.11 ± 0.249	0.211 ± 0.025
Flank face area	0.01	1.256 ± 0.156	0.125 ± 0.016
	0.02	2.506 ± 0.258	0.251 ± 0.026

process was performed with brass galvanized wire of 0.25 mm diameter, under the following electrical conditions: pulse on/off 4 μs/80 μs, discharge current 150 A, discharge voltage 160 V.

The same machining processes were applied for manufacturing of reference samples of H10S cemented carbide. For the test grinding of the rake and flank face area of BNDCC (Fig. 1) and H10S composites, diamond grinding wheels were made as follows: type 6A2 *100x10x4 D46/D25 Ba 23b*, with a reduced concentration of diamond, at *c75*, containing uncoated diamond grain manufactured by the Lands company, with a grit size of *D46*, type *LS120* (38–45 μm) and *D25*, type *LS600F* (20–30 μm), and an amorphous binder from the Al_2O_3-SiO_2-Na_2O-B_2O_3-BaO system.

3 Methods

The grinding process was carried out on a *4AM* grinding machine manufactured by FUM Pabianice and equipped with an attachment for low speed-grinding and cooling by means of spraying a 2% water solution of PGA SYNKON coolant concentrate. The fixed and variable parameters of the grinding process were established basing on the results of previous studies [8].

The following variable parameters were adopted:

- A grinding depth of 0.02: 0.01 mm/double stroke
- A diamond grain granulation of D46, D25
- Five repetition tests (5)

The following fixed parameters were adopted:

- The test stand
- The peripheral speed of grinding wheel vs 4.8 m/s
- The wheel's characteristics and dimensions: *type 6A2 100x10x4*
- The type of feed coolant: Synkon
- The coolant method: flooding

Fig. 3 The X-ray diffraction patterns obtained for BNDCC sample for the different measurement geometries—long edge (rake face), *L*, and short edge (flank face), *S*—**a** before grinding and **b** after grinding
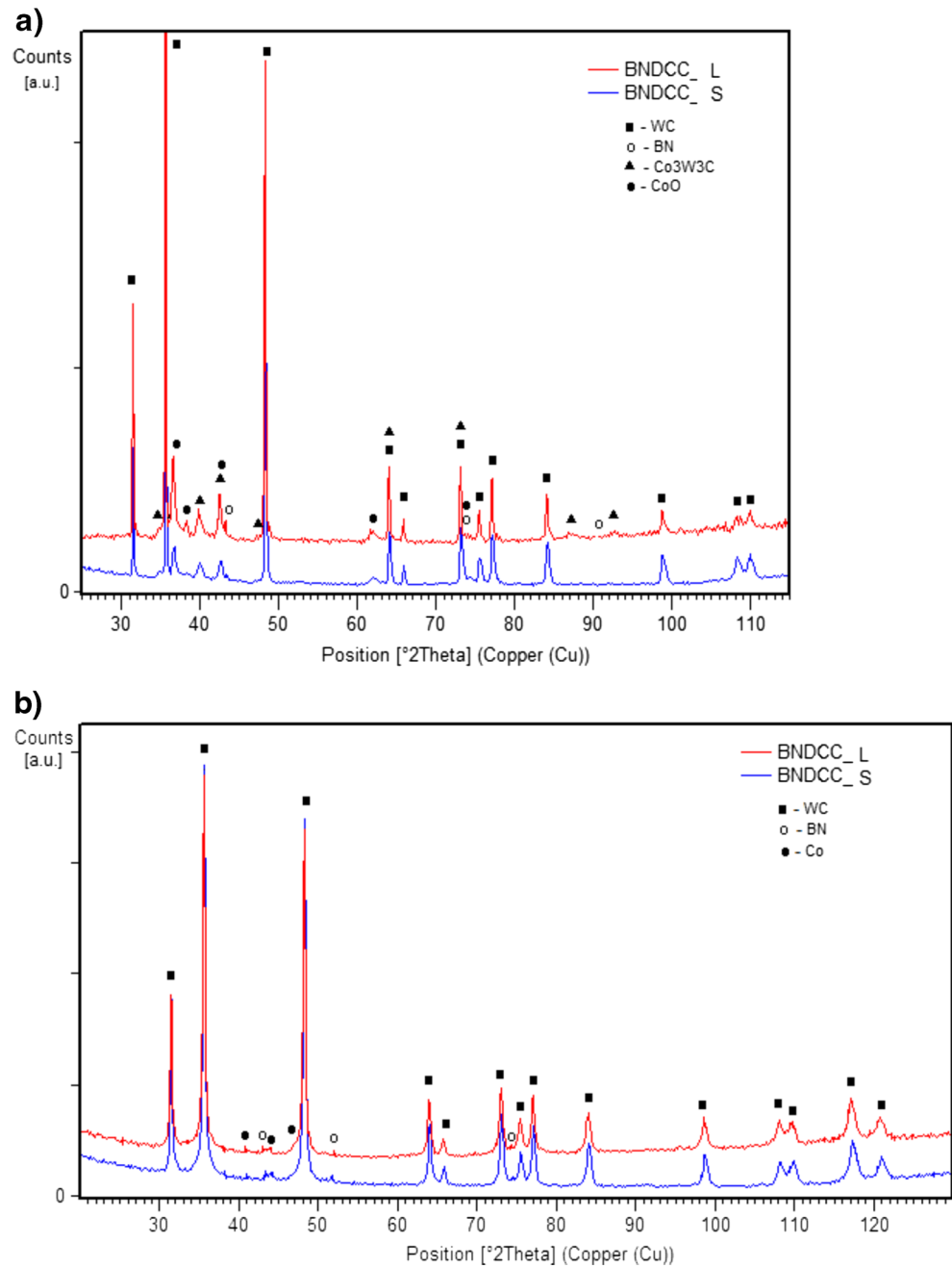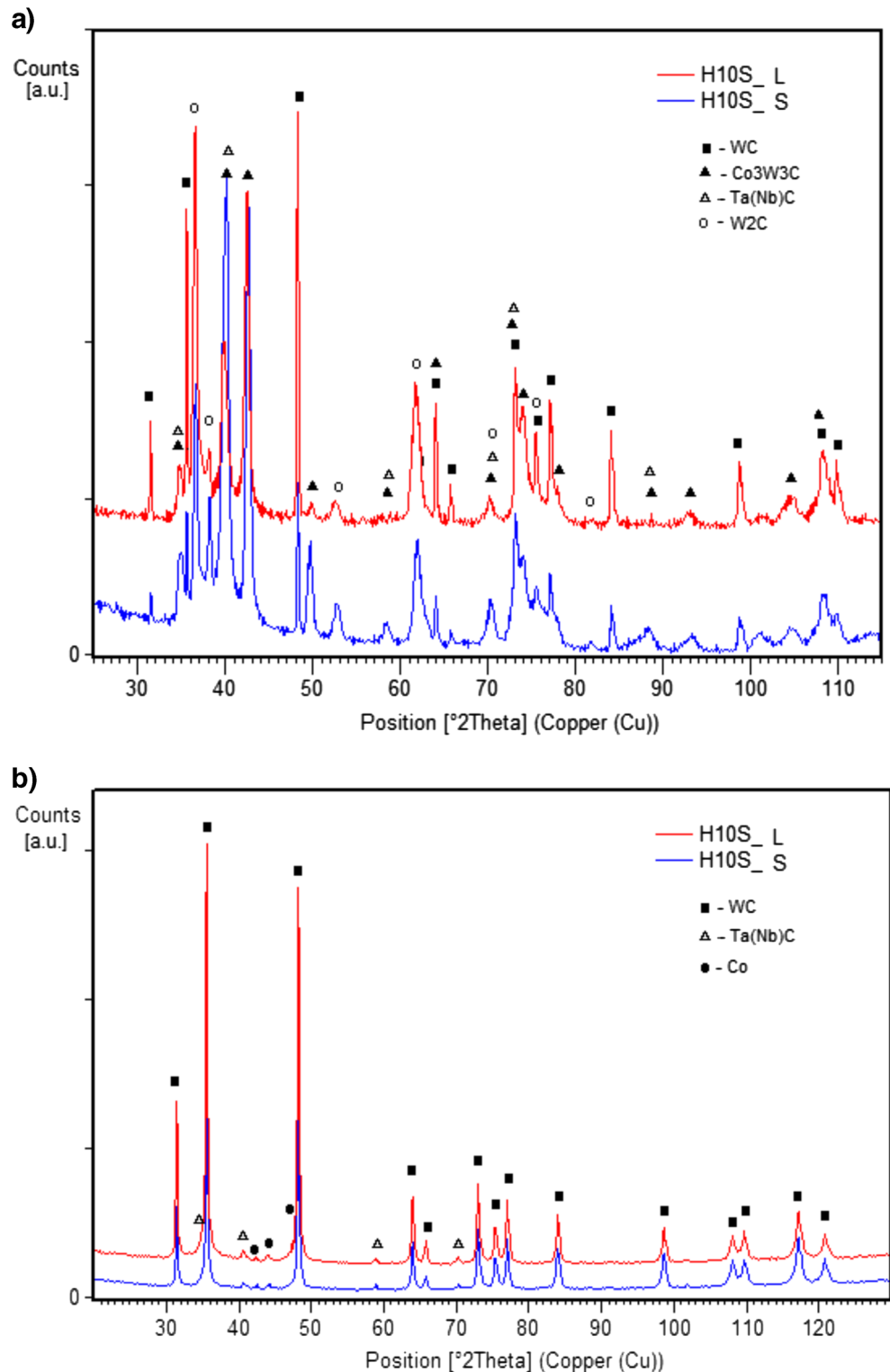

Table 6 Results of the phase analyses of the BNDCC sample before and after grinding

	Space group	Crystal system	Unit cell parameters a / b / c [Å]	Before grinding	After grinding
WC	P-6m2	Hexagonal	2.9063/2.8375	x	x
BN	F-43m	Cubic	3.6159	x	x
Co₃W₃C	Fd3m	Cubic	11.1120	x	–
CoO	Fm-3m	Cubic	4.2400	x	–
Co	P63mmc	Hexagonal	2.5054/4.0893	–	x

Fig. 4 The X-ray diffraction patterns obtained for H10S sample before grinding for the different measurement geometries—long edge (rake face), *L*, and short edge (flank face), *S*—**a** before grinding and **b** after grinding

- A testing system of 24 s for the rake face area and for 30 s for the flank face area
- The concentration of the diamond: *c75%*

Before and after the grinding process, samples were analyzed using the XRD method and the phase composition was determined. After which, the residual stress along the rake and flank face area of the composite was determined.

The weight of the material removed and the height of the wheel were measured. The volume of abraded material, the material removal rate for the grinding, by volume,

Table 7 Results of the phase analyses of the H10S sample before and after grinding

	Space group	Crystal system	Unit cell parameters a / b / c [Å]	Before grinding	After grinding
WC	P-6m2	Hexagonal	2.9063/2.8375	x	x
W$_2$C	Pbcn	Hexagonal	4.7280/6.0090/5.1930	x	–
Co$_3$W$_3$C	Fd3m	Cubic	11.1120	x	–
Ta(Nb)C	Fm-3m	Cubic	4.4500	x	x
Co	P63mmc	Hexagonal	2.5054/4.0893	–	x

namely Q_w, and the material removal rate for the grinding, per unit of active grinding wheel, Q'_w, were calculated. The weight of the samples was measured before and after each grinding process with a laboratory scale with a measurement accuracy of up to 0.001 g. The height of the wheel before and after each test was measured with electronic calipers with accuracy of 0.01 mm. Measurements of the surface topography of the BNDCC composite and the H10S reference sample H10S were taken using a TOPO 01 o1vP modular profilometer of IAMT production [10].

Topography of surfaces was measured before attempting the grinding and after its completion. The values of the surface roughness parameters (R_a, R_z, R_t) and the edge roughness parameters roughness were calculated. The microscopic observation of the flank and rake face area was carried out on a scanning electron microscope (SEM) before and after the grinding process.

The X-ray diffraction patterns were obtained using a PANalytical Empyrean diffractometer with copper radiation (λCu Kα = 1.5418 Å). The phase analysis was conducted using ICDD (PDF-4+ 2014) files. The refinement of the unit cell parameters for the studied materials was performed using the Rietveld refinement [11] with the HighScore Plus PANalytical software. The XRD measurements were taken for both surfaces, namely, the rake face (L) and the edge area (S), of the BNDCC and the H10S reference material before and after grinding. The scheme

of geometry measurement of the investigated samples is presented in Fig. 2.

The X-ray measurements for the determination of residual stress were performed using an Empyrean PANalytical diffractometer with copper radiation (λCu Kα = 1.5418 Å) at two φ angle directions, 0° and 90°, parallel with, and perpendicular to, the X-ray beam. The $sin^2\psi$ method was used in order to determine the residual stresses [14]. The Poisson coefficient (ν) and Young modulus (E) values characterizing the main WC phase, which were used during performed analyses, are 534.4 GPa and 0.22, respectively [15].

Microstructure studies of the BNDCC composite flank and rake face area of were conducted before and after the grinding process. An SEM-LV 6064 JEOL scanning electron microscope was used under the following conditions:

- An accelerating voltage of 10 kV
- The distance from the pole 10
- The character of the backscattered electrons image (BES)

4 Results and discussion

The results of the grinding process using a *D46* and *D25* diamond wheel containing the newly developed bond and

Table 8 Results of residual stress calculations (σ) obtained for WC phase (201) in the BNDCC sample for long edge (rake face), L, and short edge (flank face), S

Residual stress BNDCC		σ [MPa] WC (201)	
	Edge	0°	90°
Before grinding	L	6302	− 50
	S	− 227	− 319
After grinding	L	− 406	301
	S	− 1673	− 799

Table 9 Results of residual stress calculations (σ) obtained for WC phase (201) and H10S sample for the long edge (rake face), L, and the short edge (flank face), S

Residual stress H10S		σ [MPa] WC (201)	
		$\varphi = 0°$	$\varphi = 90°$
Before grinding	L	− 2273	− 3756
	S	− 1388	− 2205
After grinding	L	− 570	− 1577
	S	− 1005	− 1571

Table 10 Profile parameters of the flank face of BNDCC composite before and after grinding process

Profile parameters	Before grinding process		After grinding process	
	Average	Accuracy S	Average	Accuracy S
R_a [μm]	1.137	0.055	0.040	0.002
R_v [μm]	3.452	0.259	0.161	0.023
R_z [μm]	6.808	0.402	0.296	0.035
R_t [μm]	8.426	0.823	0.395	0.120

Table 12 Profile parameters of the flank face of H10S composite before and after grinding process

Profile parameters	Before grinding process		After grinding process	
	Average	Accuracy S	Average	Accuracy S
R_a [μm]	1.299	0.097	0.051	0.001
R_v [μm]	4.005	0.351	0.195	0.012
R_z [μm]	7.558	0.553	0.364	0.016
R_t [μm]	9.692	1.013	0.449	0.025

operating the tool at a peripheral speed of 4.8 m/s are presented in Tables 2, 3, 4, and 5. Presented results are averaged values of five grinding attempts.

Analysis of the results obtained from the tests leads to the conclusion that introducing a harder phase (CBN) to WCCo (BNDCC composite) did not result in significant differences in the grinding efficiency Q_w for either the D46 or the D25 grinding wheel at the same value of working engagement. This can be explained by the formation of a solid lubricant (MoS2) in contact with which significantly reduced friction. Because of total material selection, a feed rate of 0.02 mm/double stroke under this treatment is preferred. The concentration of diamond grain, at c 75, which is lower than that of standard diamond wheels, did not have a significant influence on grinding performance. In both cases (grinding with D46 and D25), the self-sharpening phenomenon involving microchunking, providing the formation of new, sharp microedges, was observed. It was explained by a very good quality of ceramic binder that allowed to keep the diamond grains until its self-sharpening.

4.1 XRD measurements

The structural analysis conducted on the basis of the Rietveld method leads to obtaining the refined values of the unit cell parameters for identified phases [12, 13]. The diffraction patterns obtained for the rake face and edge area of the samples show no significant differences in phase composition. The results of the phase analysis of

BNDCC sample before grinding are presented in Fig. 3a and Table 6. The main phases detected in the material are WC, BN, Co_3W_3C, and CoO. The phase analysis performed for the BNDCC sample after the grinding process showed the presence of WC, BN, and Co phases (Fig. 3b and Table 6). There are no lines for the Co_3W_3C and CoO phases, which indicates that they are only present on the surface of the samples. The X-ray diffraction patterns obtained for both surfaces show no differences.

Figure 4a presents the diffraction patterns obtained for the rake face and flank face of the reference material H10S before grinding. The WC, W_2C, Co_3W_3C, and Ta(Nb)C solid solution are detected. However, the differences in the intensities of the diffraction lines of the WC and W_2C phases, in a range of 35–45° 2θ, are observed. This indicates the presence of texture of them in the material. The XRD results show no significant differences in phase composition, either. The results of the phase analysis are presented in the Table 7. The phase analysis performed for the H10S sample after grinding process showed that only the WC, Ta(Nb)C, and Co phases were present (Fig. 4b and Table 7). The X-ray diffraction patterns also show no differences.

There are differences in the amounts of observed phases, which indicates a non-homogenous phase distribution on the studied surfaces.

4.2 Stress determination

Values of residual stresses in the BNDCC sample before and after grinding were calculated for WC, the main phase

Table 11 Profile parameters of the edge roughness of BNDCC composite before and after grinding process

Profile parameters	Before grinding process		After grinding process	
	Average	Accuracy S	Average	Accuracy S
R_a [μm]	1.082	0.097	0.652	0.036
R_v [μm]	3.479	0.582	2.776	0.362
R_z [μm]	7.885	0.823	4.357	0.311
R_t [μm]	11.267	1.314	6.346	0.983

Table 13 Profile parameters of the edge roughness of H10S composite before and after grinding process

Profile parameters	Before grinding process		After grinding process	
	Average	Accuracy S	Average	Accuracy S
R_a [μm]	1.636	0.178	0.431	0.058
R_v [μm]	4.525	0.597	1.880	0.055
R_z [μm]	10.717	1.518	3.292	0.463
R_t [μm]	16.553	6.578	5.259	1.574

a)

Profil   P, W, R   Filtr 0.8 mm
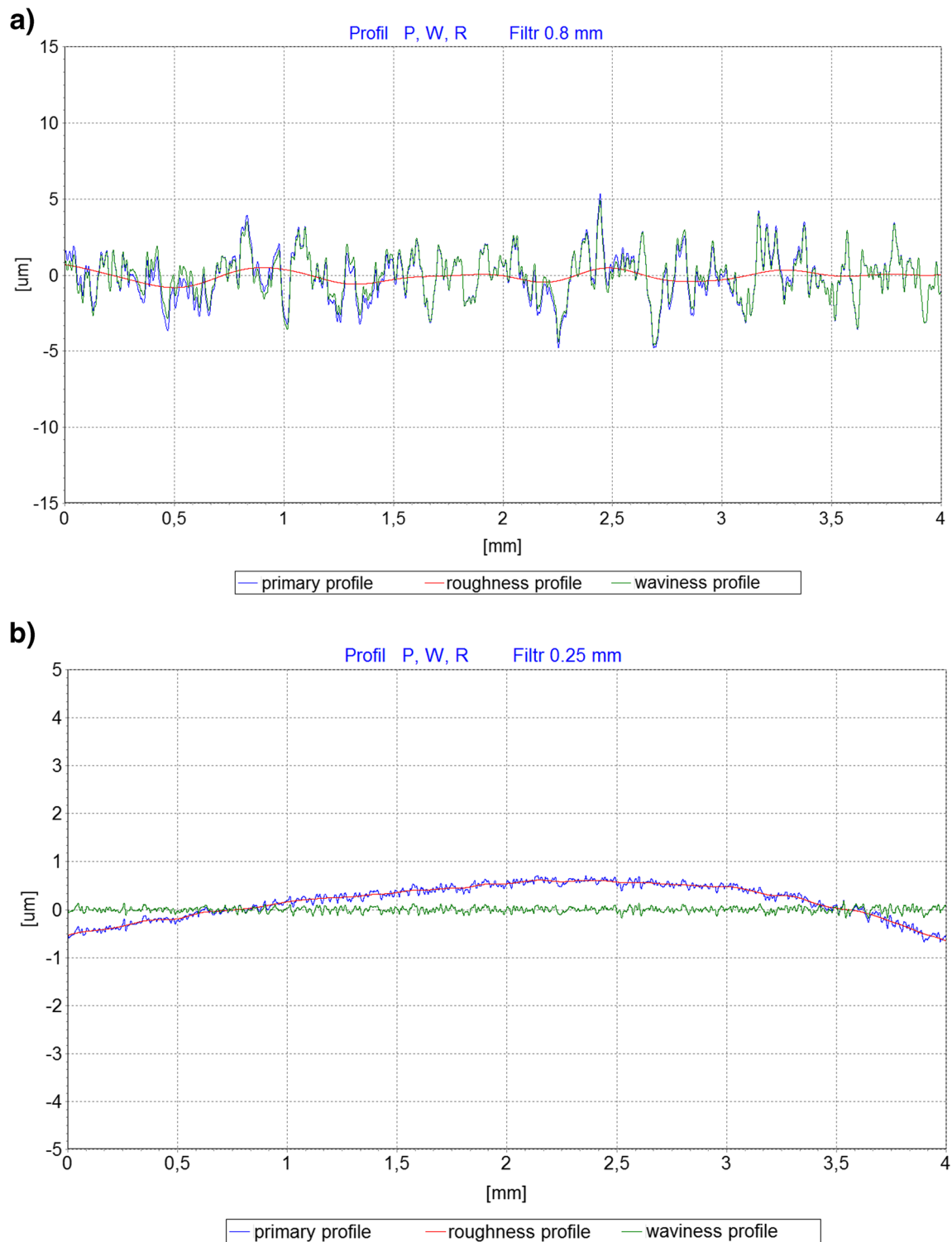
b)

Profil   P, W, R   Filtr 0.25 mm

Fig. 5 Profile of flank face of BNDCC composite **a** before and **b** after grinding process

present in the material, on the basis of the non-overlapping diffraction line $2\theta = 48.30°$, $d_{hkl} = 1.88353$ Å (101) $2\theta = 84.07°$, $d_{hkl} = 1.14875$ Å (201). The residual stresses were calculated only for matrix composite in order to observe influence of reinforcing particles on the

stress character in the final material. The residual stress results obtained for the long edge (rake face) and short edge (flank face) are presented in Table 8.

The residual stresses obtained along the short edge after grinding have compressive character. The results
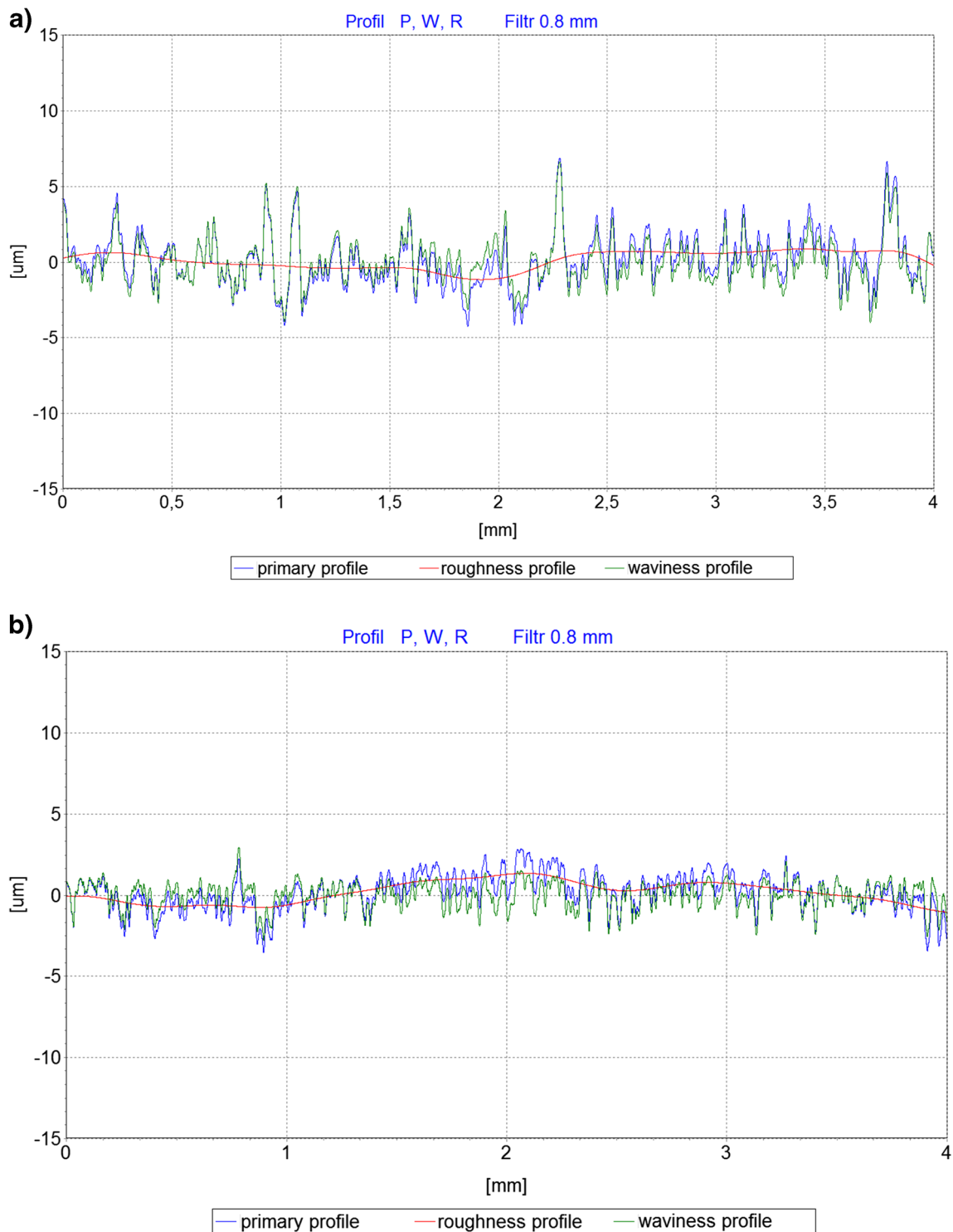
Fig. 6 Profile of edge roughness of flank face of BNDCC before and after grinding process

obtained along the rake face are of different nature. This might be an effect of applied manufacturing technology, especially the EDM machining method. During the EDM machining process, the heat is generated at the contact of the blade/material, leading to a gradient of temperature reaching into the material. The highest temperatures are located on the surface and on the cutting edge of the rake face of material, and the value decreases with distance from it. It follows that the surface layer after the EDM treatment is characterized by a state of tensile stress.

a)

b)
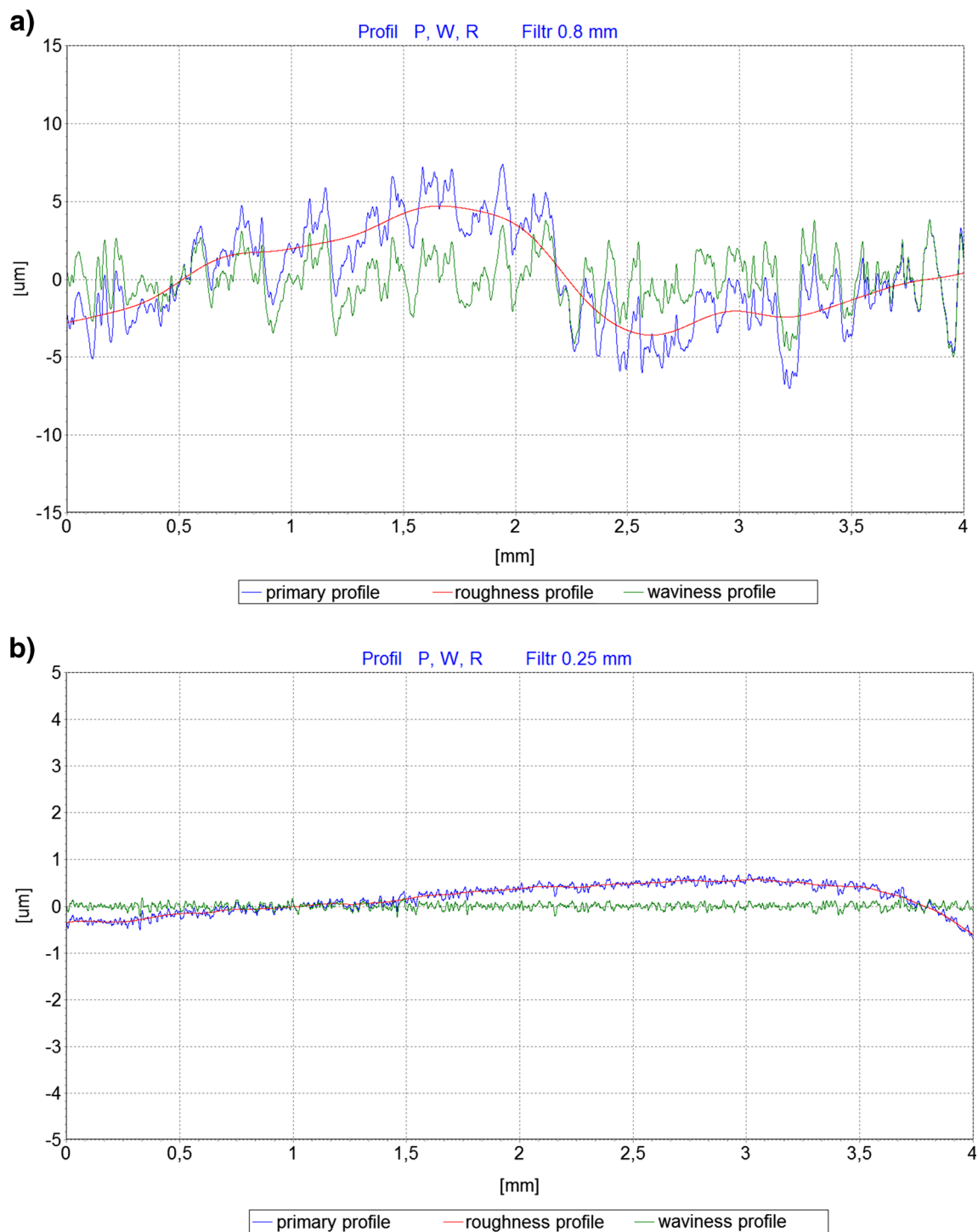
Fig. 7 Profile of flank face of H10S composite **a** before and **b** after grinding process

Applied grinding removes the top layer of the material and thus exposes the inner layer characterized by the presence of compressive stresses. Obtained results indicate also presence of non-homogeneities in the material. The residual stresses in the reference sample, both before and after grinding process on both surfaces, had compressive nature (Table 9).

4.3 The topography and microstructure of the BNDCC composite and reference sample H10S surfaces

The topography results can be explained by the specificity of the grinding process. It is related to the length of the grinding wheel's contact with the material being ground and the different values of the unit pressure of the wheel
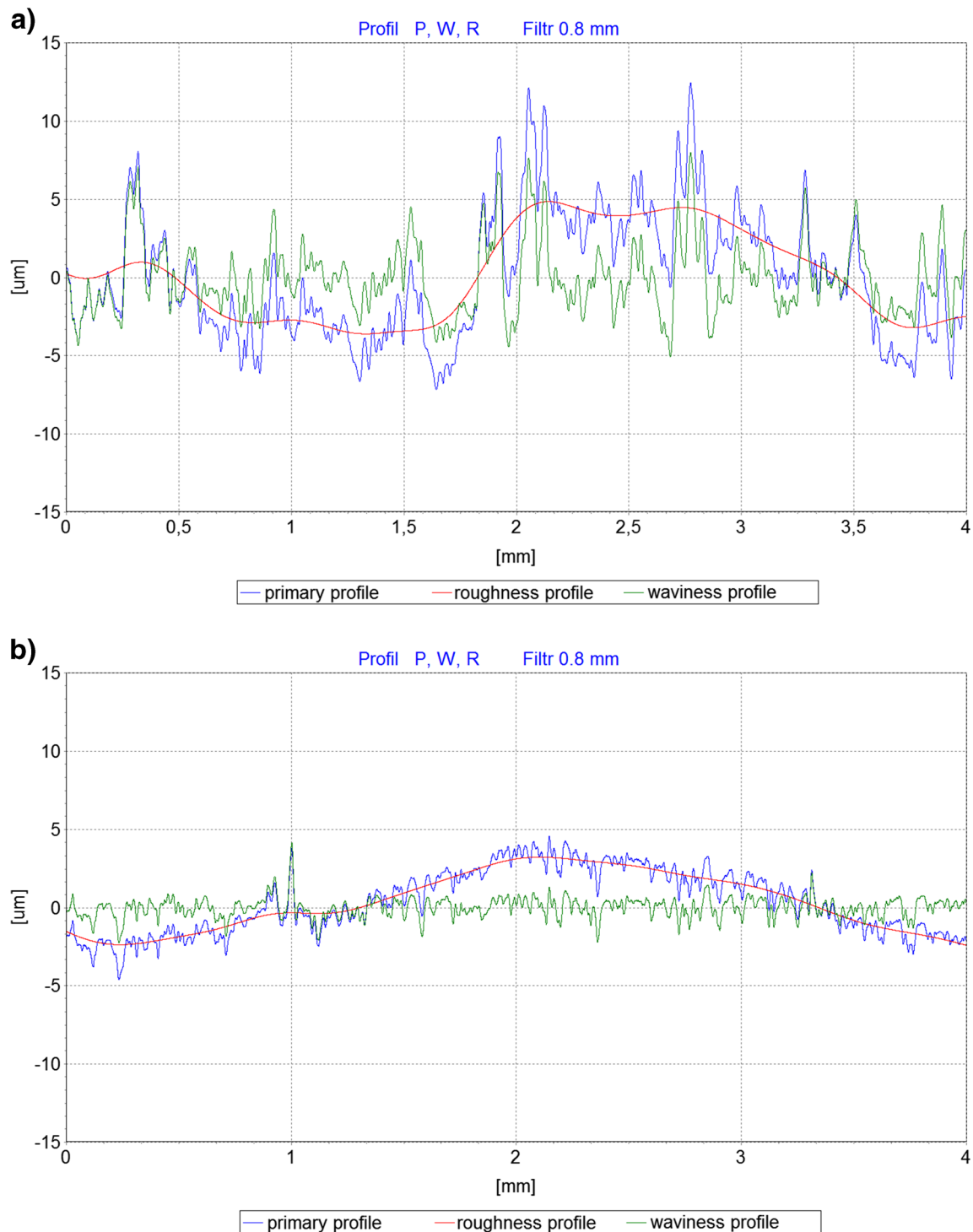
Fig. 8 Profile of edge roughness of H10S composite **a** before and **b** after grinding process

at the entrance and exit from the material. The edge roughness of the flank and rake face area of the BNDCC and H10S composites, described by roughness parameters (R_a, R_z, R_t), (Tables 10, 11, 12, and 13), had slightly higher values, mainly as a result of the size of the grinding material's contact surface.

Visualization of surface topography of tested materials is presented in Figs. 5, 6, 7, and 8. Using the correlation coefficient as the quotient of R_a before and after grinding, expressed as a percentage, it can be stated that the quality of the flank composite of both the BNDCC and the H10S improved significantly, by 2842% for the BNDCC and
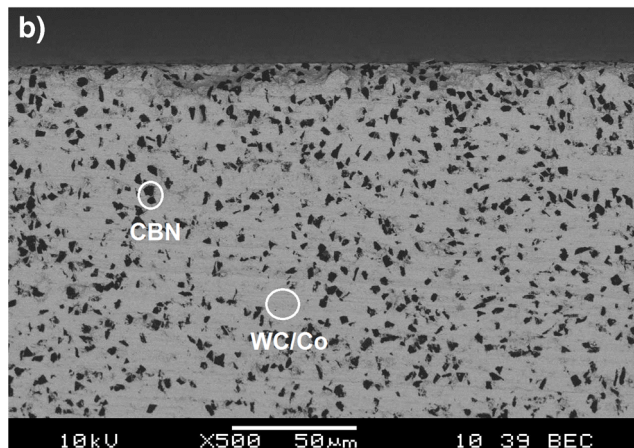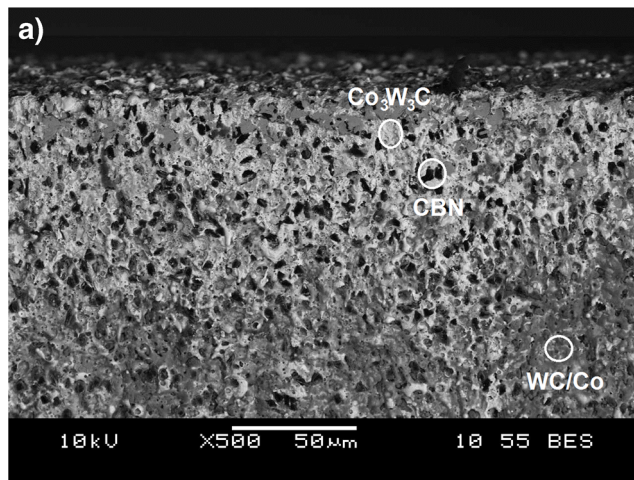
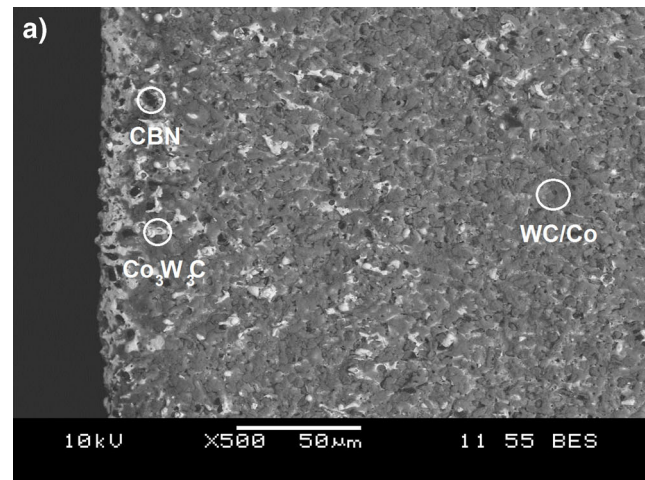Fig. 9 SEM images of rake face of BNDCC composite **a** before and **b** after grinding
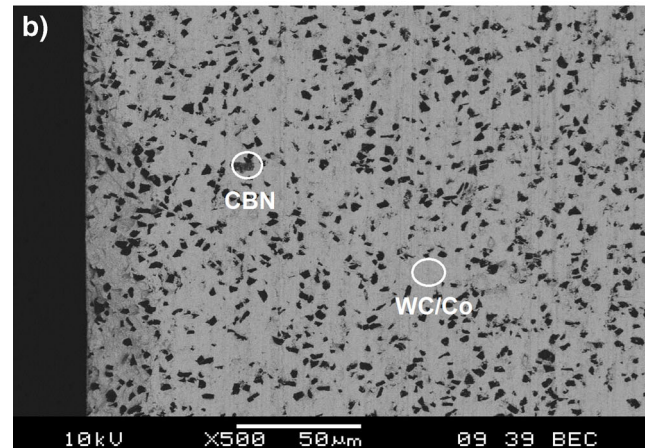
Fig. 10 SEM images of flank face of BNDCC composite **a** before and **b** after grinding

2547% for the H10S. The value of the cutting radius samples of both the BNDCC and H10S composites was slightly higher prior to the grinding process than it was afterwards, at 0.13 and 0.09 μm, respectively. There was no additional bruising, which indicates that the grinding parameters and methods of securing the samples were selected properly.

The results for the surface roughness of the flank face area and the edge roughness of the BNDCC and H10S composites are shown in Figs. 5, 6, 7, and 8, where the results of the profile analysis are presented. All the samples of the surface roughness parameters were often inferior to the output parameters. Flank face area surface of both, BNDCC composite and samples of the H10S have lower values of the parameter of surface roughness (R_a, R_z, R_t) than the rake face area.

Before grinding, microstructures of the samples had visible "white layer'" on the edges (Figs. 9a, 10a, 11a, and 12a). The presence of "white layer" results from wire EDM cutting and is created from the Co_3W_3C non-stoichiometric compound and cobalt oxide CoO. During

grinding process, that layer was removed, as was confirmed by X-ray examination (Figs. 7b and 8b). The sharp edge of the composite was visible and randomly distributed grains of cubic boron nitride stood out clearly on its surface (Fig. 9b, 10b, 11b, and 12b).

To summarize the research carried out so far, it can be concluded that the proposed conditions for grinding the flank and rake face area of both the BNDCC composite and the H10S reference sample using the diamond wheels with the newly developed ceramic binder were properly selected. The performance parameters of the material removal rate for the grinding were similar, (Q_w flank face area for the BNDCC 1.40×10^{-2} mm^3/s, Q_w flank face area of H10S 1.46×10^{-2} mm^3/s) regardless of the granularity of diamond grinding wheels (D46, D25). In both cases, the self-sharpening phenomenon, involving microchunking provided to form the new sharp microedges, was observed. Measurements of the surface topography of flank face area, rake face area, and of the edge roughness for both the BNDCC and the H10S showed that surface roughness parameters after grinding
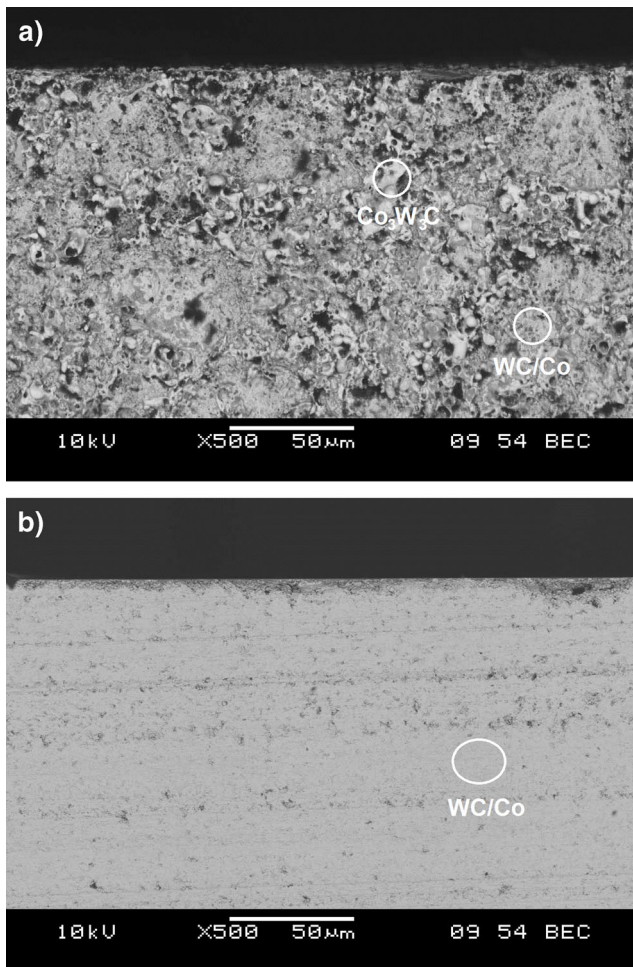
Fig. 11 SEM images of rake face of H10S composite **a** before and **b** after grinding

Fig. 12 SEM images of flank face of H10S composite **a** before and **b** after grinding

of all samples were often inferior to the output parameters. The roughness of the flank face area of both BNDCC and H10S tools had similar values to the roughness of the rake face area. Measured R_a of the BNDCC flank face area was 0.040 μm and the R_a of the H10S flank face was equal to 0.051 μm, while the roughness of the rake face edge R_a of BNDCC area was 0.117 μm and the R_a of the H10S was 0.101 μm. This can be explained by the specificity of grinding process, related to the length of contact of grinding wheel with material being ground and the different values of unit pressure at the time of entry into material of the wheel and out of the material. The sharp edge was clearly visible. Cubic boron nitride grains were visible on the composite surfaces. The residual stresses obtained along the short edge after grinding have a compressive character. The results obtained for the rake face display different characters, which might indicate non-homogeneity in the material. In general, the residual stresses in the H10S reference sample have the compressive nature on both the surfaces tested, both before and after the grinding process.
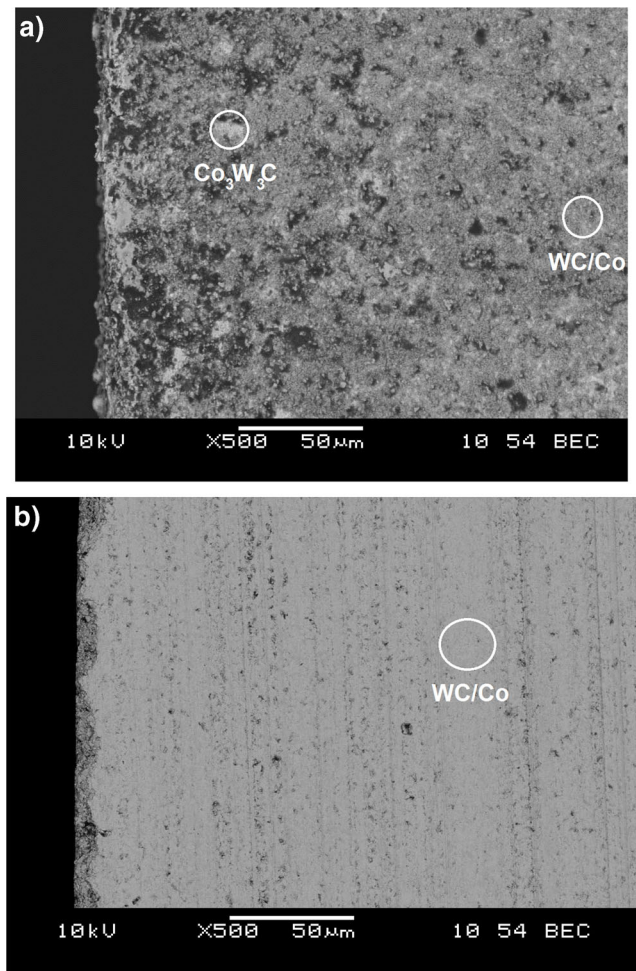
5 Conclusions

Results of performed studies and analyses proved the proper choice of grinding wheel binder material, which enables self-sharpening of the grinding wheel during grinding process, what is very useful phenomenon for proper machining. Analysis of the measured surface topography parameters clearly indicates the significant improvement after grinding in comparison to the state before the grinding process. Selected method of cutting tool manufacturing enforced existence of "white layer" (heat affected zone) on the surface of BNDCC and H10S composites before grinding. X-ray studies of that layer indicated the presence of Co_3W_3C phase. White layer was removed during the grinding process. It may be stated that binder type and tool work conditions, described in the paper, proved their usefulness in the practical application of grinding process.

References

1. Houy- G et al (2012) Effect of porosity on the grinding performance of vitrified bond diamond wheels for grinding. PCD Blades; Ceram Int 38:6215–6220. https://doi.org/10.1016/ceramint.2012304.074

2. Jackson MJ, Hitchiner MP (2013) High performance grinding and advanced cutting tools, chapter 2; Springer Science+Business Media New York. https://doi.org/10.1007/978-1-4614-3116-9

3. Kruszewski M, Rosiński M, Grzonka J, Ciupiński Ł, Michalski A, Kurzydłowski KJ (2012) Cu composites—a diamond with a high thermal conductivity produced by PPS. Ceram Mater 64:335–337

4. Rosiński M, Chrzanowski W, Spychalski M, Michalski A (2012) Wpływ parametrów procesu szlifowania na stan powierzchni kompozytu WCCo/diament wytwarzanego metodą PPS. Mater Ceram 64:314–318 (in Polish)

5. Wachowicz J, Michalski A (2014) Trwałość ostrzy skrawających z kompozytów diament/WCCo w obróbce skrawaniem płyty MDF. Mater Ceram 66:10–13 (in Polish)

6. Rosiński M, Michalski A (2012) WCCo/cBN composites produced by pulse plasma sintering method. J Mater Sci 47(20):7064–7071. https://doi.org/10.1007/s10853-012-6532-x

7. Lin K-H, Peng S-F, Lin S-T (2007) Sintering parameters and wear performances of vitrified bond diamond grinding wheels. Int J Refrac Metals Hard Mater Elsevier 25:25–31

8. Staniewicz-Brudnik B, Bączek E, Skrabalak G (2015) The new generation of diamond wheels with vitrified (ceramic) bonds; book sintering techniques of materials. Chapter 4:53–76

9. Procyk B, Staniewicz-Brudnik B, Majewska-Albin K (2001) Investigations of wettability and reactivity in glass/carbon and glass/ceramic systems, HTC–2000 High Temperature Capillarity, Third International Conference, 19-22 November, Kurashiki, Japan. Transactions of JWRI, 30, Osaka University: 149–154

10. PN-EN ISO 4287:1999 - wersja polska (polish version) - Specyfikacje geometrii wyrobów - Struktura geometryczna powierzchni: metoda profilowa - Terminy, definicje i parametry struktury geometrycznej powierzchni

11. Young RA (1993) The Rietveld method. Press, Oxford University

12. Karolus M (2006) Applications of Rietveld refinement in Fe-B-Nb alloy structure studies. J Mater Process Technol 175:246–250

13. Karolus M, Łagiewka E (2006) Structure studies of $Fe_{81}Nb_5B_{14}$ annealed alloys by Rietveld refinement. J Alloys Compd 423:92–95

14. Cullity BD (2001) Elements of X-ray diffraction. Prentice-Hall Inc, New Jersey

15. Smithells CJ, Brandes EA (1976) Metal reference book, 5th edn. Butterworths, London, pp 975–980